Synthetic Workload Generation of Broadcast Related HEVC Stream Decoding for Resource Constrained Systems

Hashan Roshantha Mendis and Leandro Soares Indrusiak
Real-time Systems Group, Department of Computer Science, University of York, York, U.K.

Keywords: HEVC, Decoding, Workload Characterisation, Synthetic Workload Generation.

Abstract: Performance evaluation of platform resource management protocols, require realistic workload models as input to obtain reliable, accurate results. This is particularly important for workloads with large variations, such as video streams generated by advanced encoders using complex coding tools. In the modern High Efficiency Video Coding (HEVC) standard, a frame is logically subdivided into rectangular coding units. This work presents synthetic HEVC decoding workload generation algorithms classified at the frame and coding unit levels, where a group of pictures is considered as a directed acyclic graph based taskset. Video streams are encoded using a minimum number of reference frames, compatible with low-memory decoders. Characteristic data from several HEVC video streams, is extracted to analyse inter-frame dependency patterns, reference data volume, frame/coding unit decoding times and other coding unit properties. Histograms are used to analyse their statistical characteristics and to fit to known theoretical probability density functions. Statistical properties of the analysed video streams are integrated into two novel algorithms, that can be used to synthetically generate HEVC decoding workloads, with realistic dependency patterns and frame-level properties.

1 INTRODUCTION

HEVC (H.265) as well as its predecessor, H.264, both utilise advanced video coding techniques to efficiently compress highly dynamic and diverse video streams. Advanced compression techniques such as the use of hierarchical B-frame structures (Sullivan et al., 2012), random-access profiles (Chi et al., 2013) and scene-change detection (Eom et al., 2015), makes video decoding workloads highly variable and complex. As video streaming workloads become more sophisticated, efficient platform resource management mechanisms and optimised scheduling of tasks and are required at the decoder to optimise performance. Input workloads highly influence the simulation based evaluation of these resource management protocols, therefore it is crucial to achieve an analytical, tractable and realistic, model or abstraction of the actual application. For example, in research where workload properties such as task execution costs are assumed to be Uniform/Gaussian distributed (e.g.(Yuan and Nahrstedt, 2002; Mendis et al., 2015)), the performance evaluation might significantly deviate from the results obtained using a realistic workload with a non-uniform distribution (e.g. skewed/long-tailed).

HEVC frames are logically structured as coding tree blocks (CTB) and each CTB is recursively subpartitioned into coding units (CU) in a quad-tree manner (illustrated in Figure 1). The CU defines a region sharing the same prediction mode (e.g., intra and inter). This work, analyses traces from real HEVC decoding workloads at the group of pictures (GoP), frame and CU levels. Workload generation algorithms are presented, that use statistical distribution models that closely represent video decoding workload characteristics. Frame decoding time is derived in a bottom-up manner by utilising CU-level characteristics.

Novel Contributions: This work introduces algorithms, that can be used to generate directed acyclic graph (DAG) based HEVC decoding workloads, with statistical properties closely matching real HEVC video streams. These synthetically generated, abstract workloads can then valuable in simulation-based design space exploration research (such as in (Mendis et al., 2015; Kreku et al., 2010)), to investigate timing and performance properties more accurately. To our knowledge this is the first work to characterise HEVC decoding workloads at the block-level as well as capturing the properties of GoP-level task graphs dependency patterns, for different types of video streams.

Mendis, H. and Indrusiak, L.
Synthetic Workload Generation of Broadcast Related HEVC Stream Decoding for Resource Constrained Systems.
DOI: 10.5220/0005953200520064
In *Proceedings of the 13th International Joint Conference on e-Business and Telecommunications (ICETE 2016) - Volume 5: SIGMAP*, pages 52-64
ISBN: 978-989-758-196-0

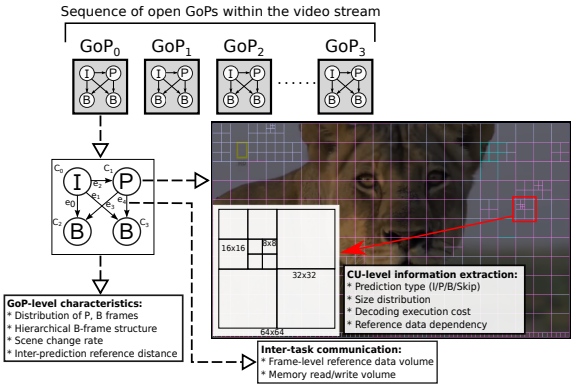

Figure 1: Task-graph based HEVC decoding workload. Workload characterisation at different levels: taskset (GoP), task (frame) and inter-task communication (reference data).

A group of pictures (GoP), represented via a DAG based application model is shown in Figure 1. There are essentially three kinds of frames in a GoP: I-frames (intra-predicted), P-frames (uni-directional, inter-predicted) and B-frames (bi-directional, inter-predicted). Inter-predicted, P and B frames use reference data from other frames in the GoP to construct the current frame. In this work, a *task-graph* (TG) refers to the graph derived from the GoP structure, where nodes in a TG refers to HEVC frame decoding tasks and edges in a graph represents inter-prediction frame data-dependencies. For example, the weight of edge $P \leftarrow I$ represent the overall decoded I-frame data that is referenced by the P-frame. Video decoding workloads are increasingly dynamic with highly varying frame decoding execution costs and dependency relationships based on the temporal and spatial characteristics of the video streams. Most specially in HEVC each inter-predicted frame can have up to 16 reference frames. Hence for example in a 35 frame GoP, there could be up to 35×16 edges in the TG and buffer requirements would vary greatly as well.

This work explores the following workloads characteristics of different video streams:

- **Taskset/GoP Characteristics:** number of P and B frames in a GoP, TG dependency characteristics, scene-changes, reference frame distribution.
- **Task/Frame and CU Level Characteristics:** decoding time and frame-to-CU relationship analysis, CU-size and type distributions.
- **Inter-task Communication Characteristics:** reference data volume per frame/CU-type (i.e. task communication traffic) and encoded frame size analysis (i.e. task memory read traffic)

2 RELATED WORK

In previous research, video decoding workloads have primarily been characterised at the *functional level*. Functional computation units of the video decoder such as entropy decoding, motion compensation, filtering, inverse quantisation etc. are identified and considered as tasks with data dependencies. A comprehensive discussion of the computation cost of the HEVC decoding functional units on ARM and x86 platforms have been given by Bossen et al. (Bossen et al., 2012). They show that motion compensation and entropy decoding dominate the decoding time of a random-access video stream. Holliman et al. (Holliman and Chen, 2003), analyse MPEG-2 and H.264 decoding workloads from a system architecture perspective by investigating how CPU branch predictions, cache and main memory hierarchy effects execution time. An abstract workload model of a parallel H.264 decoder is introduced in the MCSL benchmark framework (Liu et al., 2011). They specify the decoder functional unit execution cost and inter-task communication traffic as actual traces obtained from recorded real video streams as well as data derived from statistical properties of trace-data. However, their workload properties such as execution cost, release patterns, inter-task traffic volumes are assumed to be Gaussian distributed, which may not be accurate with the real underlying distribution.

Video decoding workloads have also been analysed at the data-level, where a task can be considered as decoding video streams at at different levels of granularity (e.g. GoP/frame/slice/block etc.). The data communication between the tasks represent reference data. Encoded frame sizes have been assumed to follow a Gamma, Lognormal or Weibull distribution (Mashat, 1999; Krunz et al., 1995). Tanwir et al.(Tanwir and Perros, 2013) in their survey paper, show that wavelet-based models offer a reasonable compromise between complexity and accuracy to model frame sizes, and the model prediction results can vary significantly based on the type of encoding. Frame decoding time is assumed to have a linear relationship with the frame size (Bavier et al., 1998). However, Isovic et al. (Isovic et al., 2003) show that there is a large variance in the decoding time for the same frame size. Roitzsch et al. (Roitzsch and Pohlack, 2006) estimates the total decoding time of a frame by adding macroblock and frame-level metrics into video stream headers at the encoder-end. In more recent work, Benmoussa et al. (Benmoussa et al., 2015) uses a linear regression model to illustrate the relationship between bit rate and frame decoding time. High variability in decoding times are seen for

Figure 2: Video sequence snapshots.

I/P/B frame-types due to different coding tools in each type and memory access patterns (Alvarez et al., 2005). Therefore, classification based on frame type need to be addressed in the model in order to obtain an accurate representation of video decoding workloads.

To our knowledge this is the first work to present characterisation and analysis of HEVC decoding at the CU-level, for different types of video streams. Unlike previous work, we analyse the reference frame patterns within a GoP as well as frame/block level decoding times. We provide algorithms that construct HEVC GoPs and frames using a bottom-up methodology by using characteristics derived at the CU-level.

3 VIDEO SEQUENCE AND CODEC TOOL SELECTION

The video sequences under investigation has been chosen to represent varying levels of spatial and temporal video characteristics. Below are the video sequences selected for this study (snapshots presented in Figure 2):

- **FastFurious5** (Action, 720p, 30fps, 15mins): Heavy panning/camera movement, frequent scene changes.
- **LionWildlife** (Documentary, 720p, 30fps, 15mins): Natural scenery, medium movement scenes, fade in/out, grayscale to colour transitions.
- **Football** (Sport, 720p, 30fps, 15mins): camera view mostly on field, camera panning, occasional close-ups on players/spectators. Large amounts of common single colour background, combined text and video.
- **ObamaSpeech** (Speech footage, 720p, 24fps, 10mins): Constant, non-uniform background; uni-camera and single person perspective, head-/shoulder movement.
- **BigBuckBunny** (CGI/Animation, 480p, 25fps, 9mins): Wide range of colours, moderate scene changes.
- **ColouredNoise** (Pseudo Random coloured pixels, 720p, 25fps, 10mins): Low compression, useful for analysing *worst-case* characteristics of a codec.

3.1 Encoder and Decoder Settings

The video streams were encoded using the open source x265 encoder (v1.7) (Multicoreware, 2015). x265 has shown to produce a good balance between compression efficiency and quality (Zach and Slanina, 2014; Naccari et al., 2015), by incorporating several advanced coding features such as adaptive, hierarchical B-frame sequences. The default settings of x265 (Multicoreware, 2015) are complimented with additional settings (Listing 1), to suit resource-constrained decoding platforms (e.g. set-top box, smart phone), targeted at broadcast/video streaming applications. Main memory data traffic of dependent picture buffer (DPB) access has shown to impact real-time display of high definition (HD) video sequences (Soares et al., 2013). Furthermore, multiple reference frames can linearly increase the memory usage of the decoder (Saponara et al., 2004). Therefore, inter-prediction has been restricted to 1 forward and 2 backward references. Higher number of B-frames in a GoP offers better compression but decreases inter-frame compression and quality (Wu et al., 2005). To strike a balance, the encoder was configured to use a maximum of 4 contiguous B-frames.

Listing 1: x265-encoder and OpenHEVC-decoder command-line arguments.

```
Encoder:
x265 --input vid_raw.yuv -o vid_enc.bin -I 35
--b-adapt 2 --bframes 4 --no-weightp --no-
    weightb
--no-open-gop --b-intra --ref 2 --csv-log-level
    2 --csv vid_stats.csv --log-level 4
Decoder:
ohevc -i vid_enc.bin -f 1 -o vid_dec.yuv -p 1 -n
```

Key-frames (random access-points in the video) provide the ability to move (e.g. fast-forward/pause/rewind) within a video stream. x265 by default treats all I-frames as key-frames if the closed-GoP (self-contained/independent GoPs) setting is chosen. Closed-GoPs offer less compression than open-GoPs, but reduce error propagation during data losses, hence more suited for broadcast video. To ensure a balance between compression and random-access precision, maximum I-frame interval of 35 frames was chosen. Weighted prediction was disabled to increase decoder performance and B-frames were allowed to have intra-coded blocks in order to be efficient during high motion/scene-change

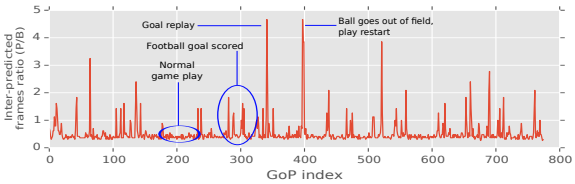

Figure 3: Ratio of P:B frames within a GoP for (*Football* video).

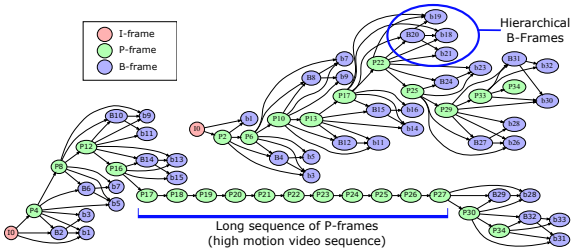

Figure 4: Example structure of a GoP (from *BigBuckBunny*). Top: low number of P-frames, Bottom: high number of P-frames. (NB: edges and nodes are unweighted).

sequences.

Decoding execution trace data was obtained using the open source, OpenHEVC (Opensource, 2015; Hamidouche et al., 2014) decoder with the minimal settings (Listing 1). In order to eliminate any inter-thread communication and synchronisation latencies which might affect decoding time data capture, for this work, multi-threading has been disabled. The platform used for decoding was a laptop with Intel Core i7-4510U 2.00GHz CPU, 4MB L3-cache and 8GB of DDR3 RAM.

4 GoP STRUCTURE MODEL

The GoP structure is directly related to the scene changes and motion in the video. For example, the ratio of the number of P and B frames per GoP (denoted as P/B ratio) of the *Football* changes with respect to high-motion scenes/scene-changes (Figure 3). We measure the scene change rate as $1/GoP_{diff}$, where GoP_{diff} refers to the mean number of GoPs between scene change events. The scene change rate in each tested video stream is given in Table 1. This metric gives a notion of how often the GoP structure changes with respect to time. *FastFurious5* has the highest scene change rate while the *Football* video has the lowest. P-frames give higher compression than I-frames, hence during scene changes, the x265 encoder increases the P/B ratio, whilst keeping the GoP length constant. Figure 4 shows two example GoPs from the *BigBuckBunny* video; the bottom GoP refers a high-motion scene (more P-frames).

4.1 Distribution of Different Frame Types

The number of P and B frames in a GoP for each video sequence is shown as a histogram in Figure 5. The number of P-frames in a GoP (denoted nP) is modelled as an exponentiated-Weibull (exp-Weibull) distribution (Mudholkar et al., 1995), where the probability density function (PDF) of the exp-Weibull distribution is given as Eq. 1 with shape parameters a and c. Additional *scale* and *location* parameters defines the relative size and position of the PDF; they are specific to the statistics package used (i.e. SciPy).

$$f(x) = ac\,(1-\exp -x^c)^{a-1}\exp -x^c x^{c-1} \qquad (1)$$

Gamma and Gumbel PDFs provided inaccurate fits to the distributions, motivating the use of exp-Weibull distribution due to its long-tail, right-skewed density and flexibility in shape. From Figure 5, it is clear that most of the video sequences fit the exp-Weibull distribution except for the case of *Coloured-Noise*, where no variation in the number of P or B frames is seen. Due to the constant GoP length N, the number of B-frames $nB = (N-1) - nP$, giving us an inverted distribution. For low-motion videos such as *ObamaSpeech* with no scene changes (Table 1), the P,B distributions show less variation and do not overlap; furthermore high values of c and a are seen. Video sequences with large variation in motion, long-tailed distributions are seen (e.g. *BugBuckBunny*), with a low c, a.

4.2 Contiguous B-frames & Reference Distance

The maximum number of contiguous B-frames (nB_{max}) in a GoP is an encoder parameter, which is set to 4 in our study. Figure 6 shows the proportion of different contiguous B-frames in a GoP. Low-motion videos (e.g. *ObamaSpeech*), show a high level of contiguous B-frames, while high motion videos (e.g. *FastFurious5*), the proportions are uniform. The proportion of contiguous B-frames have a direct impact to the reference distance of a frame. Reference distance (RFD) is the absolute difference between the GoP index of the current frame and its parent/dependent frame(s). Larger reference distances correlate with higher contiguous B-frames in a GoP. Higher average reference distances in a video stream, means the decoder has to keep a decoded frame longer in the DPB, which would result in high buffer occupancy and hence a larger main memory requirement.

Generally, P-frames do not refer to B-frames and if the encoder is restricted to have only 1 reference

Table 1: Scene change rate for all video sequences. GoP_{diff} refers to the mean number of GoPs between scene-changes.

VidName	Scene change rate $(1/GoP_{diff})$
FastFurious5	0.45
BigBuckBunny	0.30
LionWildlife	0.20
Football	0.05
ObamaSpeech	0.00

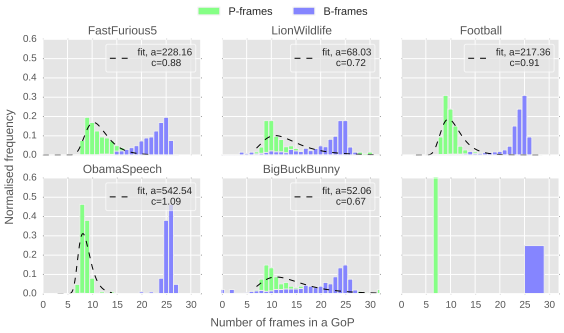

Figure 5: P,B frame histogram for all video sequences (distributions fitted to the exp-Weibull PDF with shape parameters (a, c), location=0, scale=1.5).

frame for the forward direction, then a P frame refers to the closest previous I/P frame. B-frames referred to past and future I/P/B frames with a RFD characteristic as shown in Figure 7. A highest B-frame RFD of 3 is seen as we restricted the maximum number of contiguous B-frames in the GoP to 4. Further analysis showed that a contiguous sequence of B-frames referred only to I/P-frames in close temporal proximity; therefore long edges in the task graph are not present. A correlation exists between the RFD ratios shown in Figure 7 and the number of contiguous B-frames shown in Figure 6. For example, less than 10% of of contiguous B-frames in *LionWildlife* are of size 4, which leads to a very low number of frames having a RFD of 3.

4.3 GoP Structure Generation

Construction of a synthetic GoP structure can be done in two stages as per Algorithm. 1. Firstly, a GoP sequence (in temporal decoding order) is generated, taking into account the exp-Weibull distributed P,B frames. The position of the B-frames within the GoP are uniformly distributed, but the selection of contiguous B-frame sizes are derived from the ratio relationships observed from the trace results (Figure 6). Lines 12-19 generate B-frame groups (Hierarchical B-frames) and inject them at random positions in the GoP. In phase II of the algorithm, each inter-predicted frame is assigned reference frames as per the analysis in Section 4.2. The number of reference frame

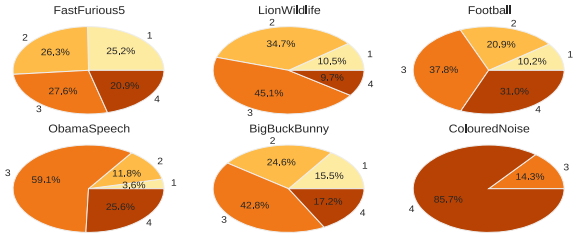

Figure 6: Number of contiguous B-frames in a GoP.

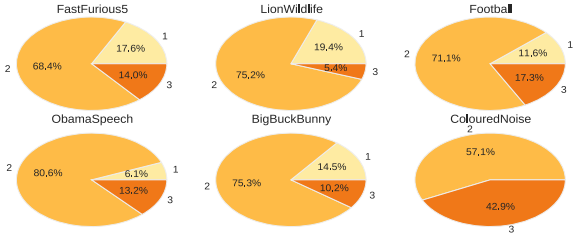

Figure 7: Reference distances for B-frames in different video sequences.

per temporal direction is an algorithm parameter. P frames are assigned the immediate previous I/P frame in the GoP. B-frames are assigned multiple reference frames (past and future) as per the RFD ratios seen in Figure 7. Lines 28, 34 and 36 derive possible and legal reference frames within the GoP. The RAND.CHOICE function, generates a random sample from the given possible reference frame set, according to the specified *probabilities* (derived from the distributions).

The parameter N in Algorithm 1 can be varied to obtain different GoP lengths. $nBmax$ and W_p can be varied to obtain different numbers of B and P frames within a GoP. rB^{fwd}_{max}, rB^{bwd}_{max} and rP^{fwd}_{max} can be used to provide more reference frames to P and B frames, this would in turn increase the number of edges in the TG. vs^{prob}_{rfd} is representative of the length of the edges in the TG and also gives a notion of the number of possible reference frames for a B-frame.

5 DERIVING A FRAME-LEVEL TASK MODEL

HEVC frames are logically partitioned into CTBs and each CTB is sub-partitioned into CUs (Figure 1). The objective of this work is to analyse the video properties at the CU granularity in order to understand and derive a frame decoding model. For example, when modelling an I-frame, a higher proportion of smaller CU sizes may need to be used, while having no P/B/Skip-CUs. A fine-grain workload characterisation can also facilitate exploration of CU/wave-

front/tile level task models as seen in (Roitzsch and Pohlack, 2006; Chi et al., 2012).

5.1 CU Sizes, Types and Decoding Time

HEVC CUs can be of the size 64x64, 32x32, 16x16, 8x8, 4x4 (intra only) and can use either intra (I-CU) or inter (P/B/Skip-CU) prediction. I-CUs refer to other CUs within the same frame and P/B/Skip-CUs refer to CUs in other frames. Skip-CUs are those which do not have a residual or motion vector, hence a reference-CU is copied directly, resulting in reduced computation complexity at the decoder and higher compression efficiency. Analysis of the CUs by size and type is necessary to derive a coarse-grain frame-level model. Figure 8 shows that intra and inter predicted frame types differ significantly in the usage of different CU sizes. There are a higher number of smaller CUs in detailed scene background videos (e.g.*ObamaSpeech* and *Football*) than others because. Overall, 64x64 CUs are least used than other sizes, however inter-frames seem to use significantly more 64x64 CUs than intra-frames. The encoder has failed to use small CU sizes for the *ColouredNoise* video.

As seen in Figure 9, except for *ColouredNoise*, all other videos contain a large proportion of Skip-CUs. The number of intra-predicted CUs (I-CU) seem to be higher in video sequences with high-motion. The inverse is true of Skip-CUs; for example in *Obamaspeech*, the amount of Skip-CUs are between 80-93%. Overall the number of P-CUs seem to be 2-3 times the amount of B-CUs, and P-frames have a higher amount of I-CUs than B-frames. The en-

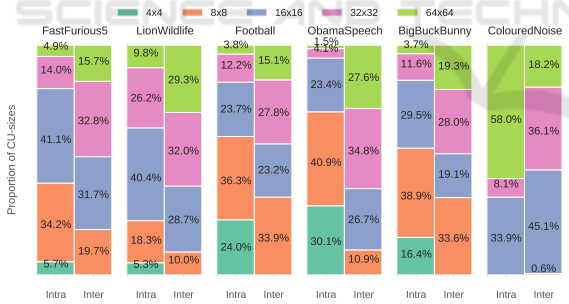

Figure 8: Proportion of CU sizes within each video sequence (per Intra/Inter frame type).

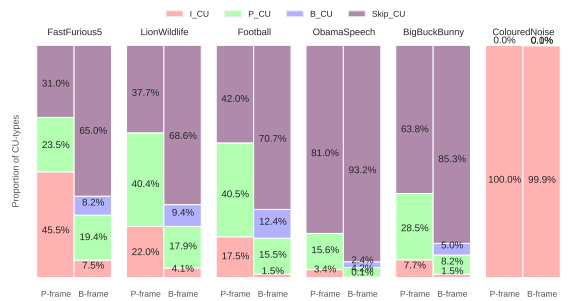

Figure 9: Proportion of CU types within each video sequence (per Inter frame type).

Algorithm 1: Pseudo-code for GoP structure construction.

Phase I - Construct GoP sequence
/* Parameter definition */
N = GoP length;
nB_{max} = max. sequential B-frames;
assert$((N-1)\%(nB_{max}+1)==0)$, validate parameters;
$nP_{min} = (N-1)/(nB_{max}+1)$;
$nP_{max} = (N-1)$, max. P-frames;
/* Contiguous B-frame probs. - Figure 6 */
$B^{prob}_{seq} = [p_0..p_{(nB_{max})}]$;
/* exp. Weibull distributed num. P,B-frames */
W_p = exp-Weibull PDF shape params: $a, c, scale, loc$
$nP = \text{EXPWEIBULL}(W_p).\text{SAMPLE}(nP_{min}, nP_{max})$;
$nB = (N-1) - nP$;
$nB_{sizes} = [1..nB_{max}]$, contiguous B-fr lengths;
/* main data structures */
$B_{fr} = \{\}$ /* hash table of positions and B-frame numbers */
$GOP_{fr} =$ "I" + ("P" $* nP$);
/* get contigous B-fr positions in the GoP */
while $\sum B_{fr}.values() < nB$ **do**
  $pos = \text{RAND.CHOICE}([1..nP], \text{prob='UNIFORM'})$;
  $tmpB_{fr} = \text{RAND.CHOICE}(nB_{size}, \text{prob=}B^{prob}_{seq})$;
  if $(B_{fr}[pos].value + tmpB_{fr}) <= nB_{max}$ **then**
    $B_{fr}[pos] += tmpB_{fr}$;
  end
end
$GOP_{fr} \leftarrow B_{fr}$ /* Put B-frames into GoP */
Phase II - Construct GoP frame references;
/* maximum frame references */
$rB^{fwd}_{max}, rB^{bwd}_{max}$ = max. forward and backward B-frame refs.;
rP^{fwd}_{max} = max. forward P-frame refs.;
vs^{prob}_{rfd} : ref. dist. ratios;
/* hash table of inter-fr references */
$fr_{refs} = \{\}$
for $fr_{ix}, fr \in GOP_{fr}$ **do**
  /* P-frames depend on prev. I/P frs */
  if $fr ==$ "P" **then**
    $r^{all\_fwd}_{POCs} = GOP_{fr}[POC < fr_{ix} \cap (r_d \leq r^{max}_d) \cap \neg$"$B$"$]$;
    $refs_{fwd} = \text{RAND.CHOICE}(r^{all\_fwd}_{POCs}, \text{size} = rP^{fwd}_{max}, \text{prob=}vs^{prob}_{rfd})$;
    $fr_{refs}[fr_{ix}] = refs_{fwd}$
  else if $fr ==$ "B" **then**
    /* B-fr depend on prev/future I/P/B frs */
    $r^{all\_fwd}_{POCs} = GOP_{fr}[POC < fr_{ix} \cap (r_d \leq r^{max}_d)]$;
    $r^{all\_bwd}_{POCs} = GOP_{fr}[POC > fr_{ix} \cap (r_d \leq r^{max}_d)]$;
    $refs_{fwd} = \text{RAND.CHOICE}(r^{all\_fwd}_{POCs}, \text{size} = rB^{fwd}_{max}, \text{prob=}vs^{prob}_{rfd})$;
    $refs_{bwd} = \text{RAND.CHOICE}(r^{all\_bwd}_{POCs}, \text{size} = rB^{bwd}_{max}, \text{prob=}vs^{prob}_{rfd})$;
    $fr_{refs}[fr_{ix}] = \{refs_{fwd}, refs_{bwd}\}$;
end

coder has failed to use inter-prediction to compress the *ColouredNoise*, where 99% of the video has been coded using intra-CUs. *BigBuckBunny* has lower amount of frame data because of the lower video resolution (480p).

The distributions of CU-level decoding time are given in Figure 10. I,P and B-CUs are fitted with a exp-Weibull distribution (parameters given in Table 2). Skip-CUs could belong to either P or B frames, and could have 1 or 2 reference CUs; hence, the Skip-CU decoding times appear to be multi-modal. They are fitted with a high-order polynomial function (coefficients given in Table 3). The large coefficient values in the model presents a risk of over fitting the data; however, we do not use the model to predict the decoding times, but randomly sample the distribution to generate new workloads. As future work, regularisation can be used to prevent over fitting.

High B-CU decoding times are due to complex transformations, in bidirectional inter-prediction. B-

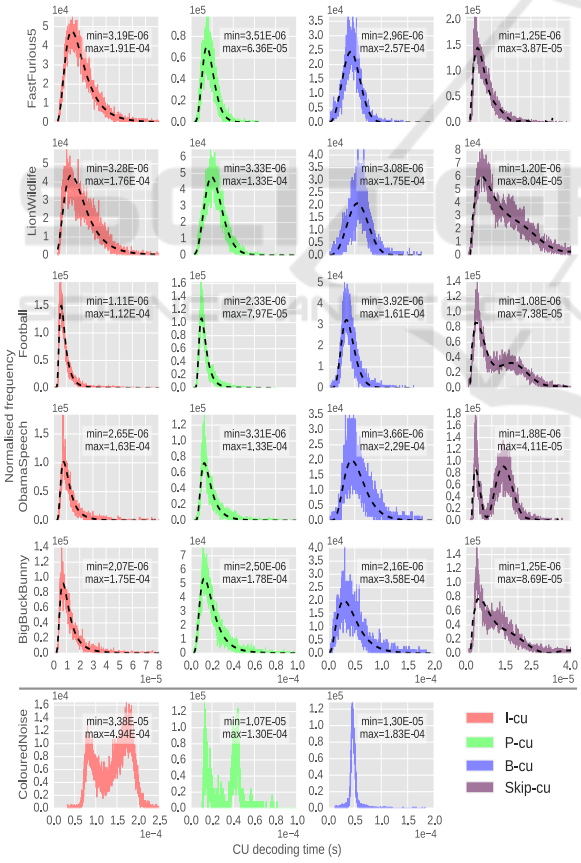

Figure 10: Normalised CU-level decoding time histogram per video sequence. I/P/B-CUs distributions fitted to a exp-Weibull PDF (dashed line; parameters given in Table 2); polynomial function fitted to Skip-CUs (parameters given in Table 3). (NB: Subfigures use different scales, share axes and distribution tails are cropped in order to assist visualisation).

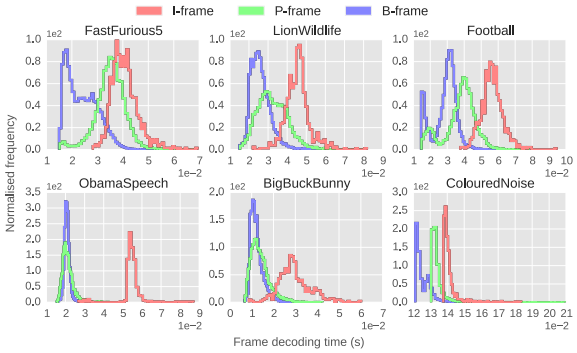

Figure 11: Normalised frame-level decoding time distribution histogram for each video sequence.

Table 2: I/P/B-CU decoding time distribution, exp-Weibull fit shape parameters. (default location=0).

CU type	a	c	scale
FastFurious5			
I-CU	1.77E+01	6.56E-01	3.05E-06
P-CU	7.47	1.28	8.42E-06
B-CU	1.38	2.55	4.51E-05
LionWildlife			
I-CU	9.24	7.43E-01	5.06E-06
P-CU	3.29	1.57	1.58E-05
B-CU	1.38	2.78	5.78E-05
Football			
I-CU	2.87E+03	3.21E-01	1.02E-08
P-CU	9.12E+02	4.46E-01	1.44E-07
B-CU	7.13	1.35	1.99E-05
ObamaSpeech			
I-CU	1.23E+03	3.25E-01	2.09E-08
P-CU	8.07E+02	3.93E-01	1.08E-07
B-CU	6.54	1.14	2.49E-05
BigBuckBunny			
I-CU	6.56E+02	3.08E-01	1.93E-08
P-CU	3.47E+01	5.62E-01	1.49E-06
B-CU	4.74	9.47E-01	1.91E-05

CUs decoding times are about 2-3 times larger than I and P-CUs. The CU decoding time is dependent on the CU-size and content of the video sequence. This is evident in the *Football* B-CU decoding times, where compared to others has a lower variance in decoding times, because of a higher proportion of inter-frame 8x8 CUs in the video stream. Furthermore, in *LionWildlife* a high amount of 16x16,32x32,64x64 CU sizes is seen, which could give rise to larger CU decoding times. Larger CU-sizes could lead to higher decoding times due to bottlenecks at the memory subsystems (Kim et al., 2012). A trend can be seen in the I-CU decoding time and the exp-Weibull shape parameters; where high-motion, high scene-change videos such as *FastFurious5* and *LionWildlife* have

a lower a and higher c, leading to wider distributions. Overall Skip-CUs have the lowest decoding time compared with the other CU-types.

The I-CU decoding time in *ColouredNoise* gave the highest execution time out of all the videos; giving an observed worst-case CU decoding time of 4.94×10^{-4} s. *Football* shows the lowest Skip-CU decoding time (1.08×10^{-6} s), which indicates that decoding CUs can have two orders of magnitude variation, depending on the type of video and CU-type and size. The CU-level decoding time data in Figure 10 correlates with the frame-level decoding time shown in Figure 11. Overall in every video stream, $t_I > t_P > t_B$ where the terms t_I, t_P and t_B denote I,P,B frame decoding times. This is mainly due to the number of Skip-CUs in a frame. E.g. a B-frame primarily contains Skip-CUs (Figure 9), and Skip-CUs decoding times are lower than other CU types, resulting in relatively lower overall B-frame decoding times. In *ObamaSpeech*, I-frame decoding is approx. 2-3 times larger than P,B-frame decoding. In FastFurious5 there is low variation between average P and I frame decoding times, this is because 45% of P-frame CUs are intra-coded. As expected it takes about 2-3 times longer to decode *ColouredNoise* when compared to the other streams, because about 99% of the stream consists of I-CUs.

5.2 Inter-task Communication Volume

In Section 4.2 the inter-frame dependency pattern in a GoP was discussed. This section investigates the volume of reference data required for inter-prediction, which is essentially the weight of each arc in the GoP-level TG. Apart from reference frame-data, the encoded frame also needs to be loaded from main memory in order to perform the decoding operations; hence this data traffic also forms part of the communication volume in the application.

The reference data is the pixel data of a decoded frame; the maximum amount of data a P-frame can reference is ($fr_{size} = (h\times w)\times bpp$), where h and w represents the frame dimensions and bpp is bytes per pixel. For B-frames this upper bound is doubled due to bi-directional prediction. Figure 12 shows the distribution of reference data categorised by direction of reference; for example $P \leftarrow I$ refers to the data referenced by a P-frame from an I-frame in the GoP. Considering the distributions and their sample sizes for each video stream, overall all inter-frames have a preferred reference probability of: $p_I > p_P > p_B$, where for example p_I denotes the probability of a frame obtaining data from an I-frame. This observation is true because B-frames have the lowest decoded

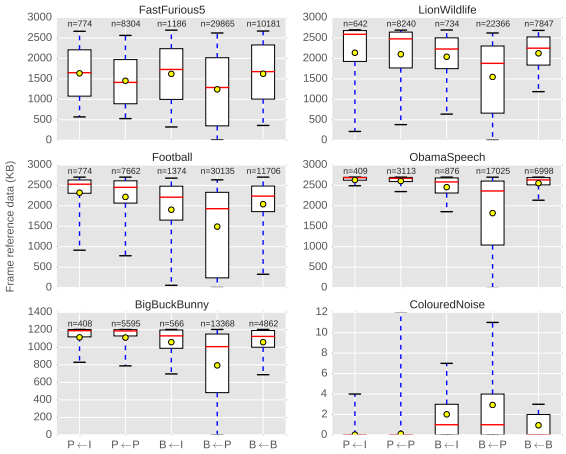

Figure 12: Distribution of frame reference data for all video sequences. E.g. $P \leftarrow I$ refers to the data referenced by a P-frame from an I-frame. Sample-size of the distribution given as n.

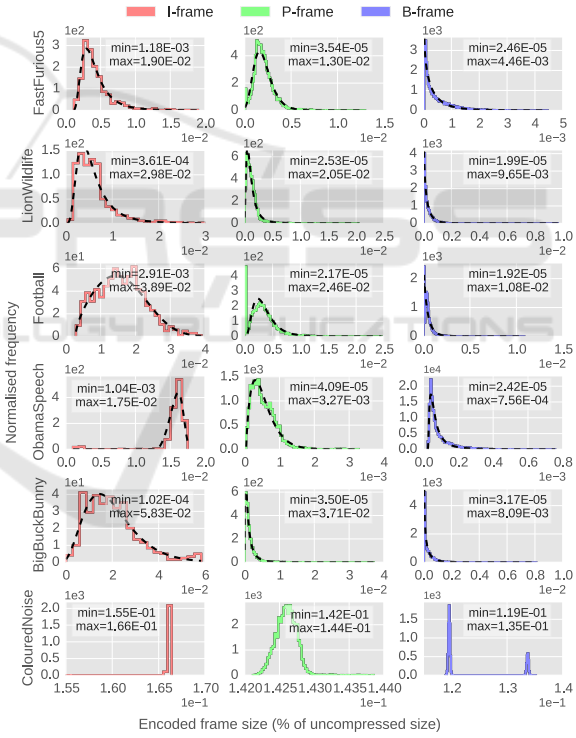

Figure 13: Distribution of frame compression ratio (encoded frame size as a % of the uncompressed frame size). Distribution fitted to Exp-Weibull PDF (dashed-line, parameters given in Table 4). (NB: Subfigures use different scales in order to assist visualisation).

frame data accuracy due to bi-directional prediction, and I-frames have the highest accuracy due only using intra-prediction. In a synthetic frame-level task generator, probabilities of reference frame selection is only required when the encoder allows the use of

more than 1 reference frame per direction. Further observations showed that when considering the total amount of referenced data per frame-type, B-frames referenced twice the amount of data than P-frames.

The reference data distributions are highly dependent on the reference frame distance (Figure 7), the number of contiguous B-frames (Figure 6) and the distribution of frame types (Figure 5) in a GoP. This is also the reason for the wide variation of reference data in the $B \leftarrow P$ distribution. The data traffic variation seems to be higher in videos with high rate of scene-change (e.g. *FastFurious5*), while the mean amount of data volume is higher in largely static videos (e.g. *ObamaSpeech*). *ColouredNoise* has very low reference data because a majority of the CUs are I-CUs.

The distribution of frame compression ratio are given in Figure 13; this data represents the size of an encoded frame. The distributions are fitted with a exp-Weibull distribution (parameters given in Table 4). Unlike in (Krunz et al., 1995) where a Lognormal distribution gave the best fit for frame-size, a right skewed distribution such as *ObamaSpeech*, does not fit a Lognormal distribution well. Overall, $s_I > s_P > s_B$, where s_I, s_P, s_B denote I/P/B encoded frame sizes. However, the long-tailed distributions tell us that there may be extreme-case scenarios where this may not always be true (further verified in (Isovic et al., 2003)). It can be observed that variation in the distribution is relative to the motion/scene-change rate of the video streams. Low-motion videos such as ObamaSpeech have a much lower encoded P/B frame size than high-motion videos. The distributions correlate with the distribution of CU-sizes and CU-types in a frame (Figure 8 and Figure 9). B-frame sizes have very long-tailed distributions compared to I or P-frames due to the variation in the number of Skip-CUs in the frame; because Skip-CUs do not contain a residual, the amount of data encoded is relatively small. In general I-frame sizes have less variation than inter-predicted frames.

5.3 Frame-level Task Generation

Algorithm 2 illustrates the frame-generation algorithm pseudocode. The algorithm builds up the frame-level task in a hierarchical bottom-up manner, by first iterating through each CTU in the frame (line 13) and then constructing a set of CUs per CTU (lines 15-32). The frame decoding time is calculated as the summation of the CU decoding time (C_{dt}) of all CUs in the frame. Videos of different resolutions can be generated by changing the N_{CTU} parameter accordingly; h, w in line 2 is the resolution of the video. For each CU in a CTU an appropriate value for the CU-type

Algorithm 2: Pseudo-code for frame construction, using CU-level properties.

```
   /* Parameter definition                                          */
 1 CTU^px_max = 64×64;
 2 N_CTU = (h×w)/CTU^px_max, number of CTUs per frame;
 3 CU_sizes = 64, 32, 16, 8, 4;
 4 CU^p_size = CU size probabilities per frame type - Figure 8;
 5 CU_types = {I-CU, P-CU, B-CU, Skip-CU};
 6 CU^p_types = CU type probabilities - Figure 9;
 7 W^I_p, W^P_p, W^B_p = expWeibull parameters: a, c, scale, loc;
 8 p^skip_c = Skip-CU polynomial coefficients;
 9 dI^lim_CU, dP^lim_CU, dB^lim_CU, dSkip^lim_CU = min/max CU dec. cost;
   /* Ref. frame selection params - Optional: if more
      than 1 ref. frames per direction.                             */
10 fr_ref = reference frames for current frame;
11 PB_rf = Prob. of current fr referencing I/P/B frames;
   /* Construct each CTU in the frame                               */
12 fr_CTUs = /* empty CTU list in frame                             */
13 for each_CTU ∈ [0..N_CTU] do
14     px = 0; CTU_CUs = {} /* init. data struct.                   */
       /* get CU-level information                                  */
15     while px < CTU^px_max do
           /* randomly select CU size                               */
16         C_s = RAND.CHOICE(CU_sizes, prob=C^p_s);
17         if (px + C_s) ≤ CTU^px_max then
18             px += (C_s)^2;
               /* randomly select CU type                           */
19             C_t = RAND.CHOICE(CU_types, prob=C^p_t);
               /* random dec. time per CU type                      */
20             if C_t == "I-CU" then
21                 C_dt = EXPWEIBULL(W^I_p).SAMPLE(dI^lim_CU);
22             else if C_t == "P-CU" then
23                 C_dt = EXPWEIBULL(W^P_p).SAMPLE(dP^lim_CU);
24             else if C_t == "B-CU" then
25                 C_dt = EXPWEIBULL(W^B_p).SAMPLE(dB^lim_CU);
26             else if C_t == "Skip-CU" then
27                 C_dt = POLYNOMIAL(p^skip_c).SAMPLE(dSkip^lim_CU);
               /* pick CU reference from reference
                  frame list                                        */
28             C_rf = RAND.CHOICE(fr_ref, prob=PB_rf);
               /* append to CU list                                 */
29             CU_info = {C_s, C_t, C_dt, C_rf};
30             CTU_CUs ← CU_info;
31         end
32     end
       /* append to CTU list                                        */
33     fr_CTUs ← CTU_CUs;
34 end
```

(line 19), CU-size (line 16), CU decoding time (lines 20-27) and CU reference frame (line 28) is selected. The selection process for these properties is facilitated by the observations and derived PDFs at the CU/frame level in Sections 5.1 and 5.2. A set of parameters (lines 1-11) needs to be carefully chosen for the algorithm, which are representative of the type of video

(e.g. high temporal activity with low number of fine-grain visual details) one intends to generate.

5.3.1 Limitations of the Workload Model

The CU type and size ratios given in Figure 10, 9 are mean results obtained at the stream-level for different frame types. In order to obtain variation of these proportions between different individual frames, we vary each percentage value according to a normal distribution. For example, when generating a frame for *FastFurious5*, rather than taking the same value (31% probability) for a SkipCU, we sample a normal distribution with $\mu = 0.31$ and $\sigma = 0.05$. The σ value needs to be high enough to add a certain level of variation between different frames of the same video stream, but not too high such that the original proportions will be masked. In real video streams however, the variation between frames would be complex and would not fit a theoretical distribution. A deeper analysis into the distribution of the CU types and sizes of a distribution of frames will need to be analysed, in order to infer the variations between frames.

Secondly, the CU decoding time provided contain latencies induced by the memory subsystems of the platform. Hence, during our evaluation we noticed the frame decoding time does not scale proportionally to the number of different CUs. In order to obtain a reasonable frame-level mode, the CU decoding time model (Figure 10) needs to be scaled down. Furthermore, the decoding time results shown in this work are dependent on the decoder implementation and our hardware architecture. The scale factors need to be tuned appropriately to suit a platform with different memory and CPU characteristics. CUs that require more memory transactions such as P/B/Skip CUs would need to be scaled down more than I-CUs. During evaluation of the generator we noticed a scale-down factor of 0.02-0.03 for I/P/B-CUs and 0.002-0.002 for Skip-CU decoding times gave satisfactory results.

6 WORKLOAD GENERATOR USAGE

As discussed in Section 1 the algorithms presented in Algorithm 1 and 2 can be used in system-level simulations to facilitate evaluation of workload resource management and scheduling techniques (e.g. (Mendis et al., 2015; Kreku et al., 2010; Yuan and Nahrstedt, 2002)). For example in (Mendis et al., 2015), we see a multi-stream video decoding application workload that needs to be allocated to multiple processing elements in order to maximise system utilisation. Figure 14 shows how the workload generators proposed in this work can be integrated into system simulators. The workload generators can be used to output task-level information (e.g. dependency patterns, execution costs, communication costs, arrival times) of a large quantity of video streams, into text-based data files (e.g. XML/CSV format) and read back in by the simulator to be used as input for system performance evaluation. The bottom-up methodology further adds flexibility into the framework, such that the CU-level information can also be used to generate HEVC tile/wave-front (Chi et al., 2013) based workloads, in a similar manner to generating frames.

As illustrated in Figure 14, a video stream can be generated by generating multiple GoPs using Algorithm 1. Within each GoP a frame can be generated using Algorithm 2. Likewise, any number of video streams can be synthetically generated and fed into a simulator. The GoP/frame-level model parameters (e.g. exp-Weibull PDF shape parameters, CU size/-type ratios), should be selected based on the type of video. Variations of videos can be generated by mixing/adapting the model parameters. For example, a high-motion video with a fine-detailed background can be generated by using a high *nP* distribution similar to *LionWildlife* (Figure 5) and using proportions of CU-sizes similar to *ObamaSpeech*(Figure 8, high 4x4, 8x8 count).

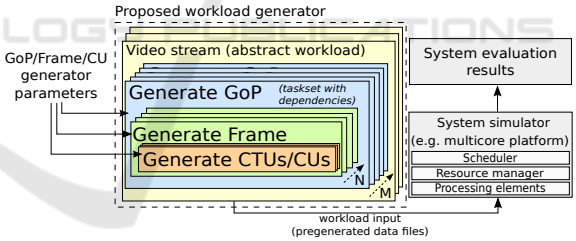

Figure 14: Integration of the bottom-up workload generator with a system simulator. (M=Number of GoPs).

Usage examples, implementation source code and analysis data has been made open to the community for reproducibility of the analyses/results and applicability of the workload generation algorithms (Mendis, 2015).

7 EVALUATION

To evaluate the proposed video decoding workloads, we synthetically generated 200 GoPs of the *LionWildlife* video stream and compared against the data gathered from the real *LionWildlife* video. From Figure 15(a) we can see that the number of P-frames in

the generated GoPs follow a exp-Weibull distribution as shown by the fit in Figure 5. However, the distribution is slightly shifted to the right causing a higher number of 4 contiguous B-frames which in turn affects the reference distance ratios. A reference distance of 3 is still the lowest, similar to the real video stream.

Figure 15(b)(left) shows the decoding time distributions of the synthetically generated frames; these need to be evaluated against the data given in Figure 11(*LionWildlife*). Due to inaccurate representation of the frame-level variations (Section 5.3.1), the distribution of the frame decoding times generated do not exactly follow the same shape as the real video stream. However, we can see that the decoding times are approximately in the same region for P and B frames (i.e between $1.0-4.0\times10^{-2}s$), which is majority of the video stream; and a slightly larger I-frame decoding time ($4.0-8.5\times10^{-2}s$) can be seen.

The difference in decoding times between P and B frames follow a similar trend to the real video stream, as P-frame decoding times are overall larger than B-frames. The generated frame decoding times show a narrower spread of values than the real video stream. We also evaluate the reference data volume distributions between the synthetically generated and real video stream. Figure 15(b)(right) shows that the $P \leftarrow I$ and $P \leftarrow P$ show a narrower spread of data volume than the real video stream. $B \leftarrow I$ results are higher than the real video and $B \leftarrow B$ show a slightly

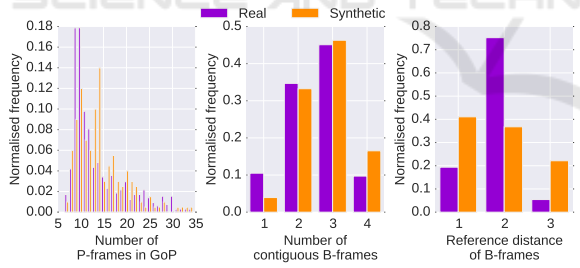

(a) GoP structure comparison: *Left*

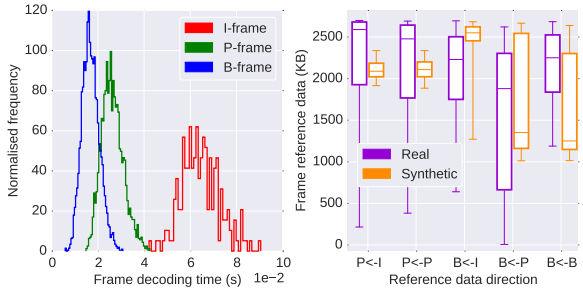

(b) Frame characteristics comparison: *Left*

Figure 15: Comparison of GoP and frame-level characteristics of a real vs. synthetically generated video stream.

Table 3: Skip-CU decoding time distribution, polynomial fit coefficients.

FastFurious5, $f(x)$=
$2.34\times10^{53}-4.62\times10^{49}x+3.87\times10^{45}x^2-1.78\times10^{41}x^3+4.84\times10^{36}x^4-7.63\times10^{31}x^5+5.82\times10^{26}x^6+4.03\times10^{20}x^7-4.09\times10^{16}x^8+2.45\times10^{11}x^9-2.99\times10^{5}x^{10}$
LionWildlife, $f(x)$=
$-8.75\times10^{49}+3.92\times10^{46}x-7.60\times10^{42}x^2+8.35\times10^{38}x^3-5.71\times10^{34}x^4+2.52\times10^{30}x^5-7.21\times10^{25}x^6+1.30\times10^{21}x^7-1.38\times10^{16}x^8+7.40\times10^{10}x^9-9.15\times10^{4}x^{10}$
Football, $f(x)$=
$-8.54\times10^{50}+3.41\times10^{47}x-5.87\times10^{43}x^2+5.71\times10^{39}x^3-3.43\times10^{35}x^4+1.32\times10^{31}x^5-3.24\times10^{26}x^6+4.90\times10^{21}x^7-4.22\times10^{16}x^8+1.75\times10^{11}x^9-1.82\times10^{5}x^{10}$
ObamaSpeech, $f(x)$=
$5.45\times10^{52}-4.99\times10^{48}x-3.55\times10^{44}x^2+7.47\times10^{40}x^3-4.81\times10^{36}x^4+1.65\times10^{32}x^5-3.32\times10^{27}x^6+3.93\times10^{22}x^7-2.61\times10^{17}x^8+8.51\times10^{11}x^9-9.65\times10^{5}x^{10}$
BigBuckBunny, $f(x)$=
$-1.13\times10^{50}+5.22\times10^{46}x-1.04\times10^{43}x^2+1.16\times10^{39}x^3-8.05\times10^{34}x^4+3.58\times10^{30}x^5-1.03\times10^{26}x^6+1.84\times10^{21}x^7-1.92\times10^{16}x^8+9.95\times10^{10}x^9-1.16\times10^{5}x^{10}$

Table 4: Encoded frame size distributions, exp-Weibull fit shape parameters.

Frame	a	c	loc	scale.
FastFurious5				
I-Fr	4.76E+01	5.15E-01	5.81E-04	1.93E-04
P-Fr	1.57E+01	7.90E-01	2.71E-05	4.41E-04
B-Fr	1.29	7.38E-01	2.46E-05	3.08E-04
LionWildlife				
I-Fr	1.31E+02	4.50E-01	0.00	1.52E-04
P-Fr	1.20E+01	5.07E-01	0.00	1.27E-04
B-Fr	1.17	7.79E-01	1.99E-05	2.47E-04
Football				
I-Fr	6.05E-01	2.74E+00	2.74E-03	1.81E-02
P-Fr	4.15	9.49E-01	1.45E-04	1.56E-03
B-Fr	1.16	8.88E-01	1.92E-05	4.15E-04
ObamaSpeech				
I-Fr	4.56E-01	6.21E+00	1.29E-02	3.69E-03
P-Fr	1.60	1.18E+00	3.79E-05	4.17E-04
B-Fr	8.45E+01	2.66E-01	2.31E-05	1.10E-07
BigBuckBunny				
I-Fr	3.36	1.23	0.00	1.39E-02
P-Fr	5.51	4.59E-1	2.23E-05	1.70E-04
B-Fr	9.80E-01	7.34E-01	3.17E-05	2.57E-04

lower distribution. However the inter-quartiles of the real and synthetic video distributions overlap, specially in the case of $B \leftarrow P$. These discrepancies are also a result of the differences in B-frame reference distances (Figure 15(a)(right)) and also the limitation of getting an accurate view of the inter-frame CU variations.

8 CONCLUSION

The aim of this paper was to characterise the workload of HEVC decoding at the GoP, frame and CU level. The state-of-the-art in video stream workload modelling, either assumes Gaussian distributed random properties such as frame decoding times and dependent data volumes or tries to estimate the decoding times with respect to frame sizes. Furthermore data dependency patterns (i.e. GoP structure patterns) are not addressed in the state-of-the-art. In this work, a bottom-up workload generation methodology is presented where, block-level characteristics were used to derive higher-level properties such as frame execution costs and reference data volumes. This work attempts to generate video decoding workloads with real statistical properties obtained from profiled video decoding tasks. It was found that frame-level decoding time correlated well with the CU-level statistics obtained. This work quantitatively shows that the inter-frame dependency pattern of the GoPs are highly correlated with the level of activity or motion in the video stream. Algorithms were presented to generate the GoP sequence and structure as well as frame generation which satisfy the probability density of real video streams.

The exponential Weibull distribution was fit to the distribution of the number of P/B frames in a GoP, CU-level decoding time and encoded frame sizes. To represent the multi-modal nature of Skip-CU decoding times, higher-order polynomial functions were chosen. Characteristics of different types of video streams including high/low activity and coarse/fine level detail imagery was analysed. The workload generation algorithms presented can be used as an input to system-level simulators. The evaluation of the proposed technique showed that the workload generators do not fully capture the extreme variations between frames. However, the average-case properties of real-video streams and synthetically generated streams are comparable.

As future work, firstly, we hope to analyse the frame-level variations and in more detail to improve the accuracy of the synthetic workload. Secondly, the relationship between the workload model and the experimental platform (e.g. decoder configuration, memory and processor architecture etc.) will need to be further analysed to derive a robust generator. Furthermore, the workload generator would need to be evaluated with higher resolution videos (e.g., 1080p or 4k) and high frame rates (e.g. 60 fps).

ACKNOWLEDGEMENT

We would like to thank the LSCITS program (EP/F501374/ 1), DreamCloud project (EU FP7-611411) and RheonMedia Ltd.

REFERENCES

Alvarez, M., Salami, E., Ramirez, A., and Valero, M. (2005). *A performance characterization of high definition digital video decoding using H.264/AVC*, pages 24–33.

Bavier, A. C., Montz, A. B., and Peterson, L. L. (1998). Predicting mpeg execution times. In *ACM SIGMETRICS Performance Evaluation Review*, pages 131–140. ACM.

Benmoussa, Y., Boukhobza, J., Senn, E., Hadjadj-Aoul, Y., and Benazzouz, D. (2015). A methodology for performance/energy consumption characterization and modeling of video decoding on heterogeneous soc and its applications. *Journal of Systems Architecture*, pages 49–70.

Bossen, F., Bross, B., Suhring, K., and Flynn, D. (2012). HEVC complexity and implementation analysis. *IEEE TCSTV*, 22:1685–1696.

Chi, C. C., Alvarez-Mesa, M., Juurlink, B., Clare, G., Henry, F., Pateux, S., and Schierl, T. (2012). Parallel scalability and efficiency of HEVC parallelization approaches. *IEEE TCSVT*, 22:1827–1838.

Chi, C. C., Alvarez-Mesa, M., Lucas, J., Juurlink, B., and Schierl, T. (2013). Parallel HEVC decoding on multi and many-core architectures: A power and performance analysis. *Journal of Signal Processing Systems*, 71:247–260.

Eom, Y., Park, S., Yoo, S., Choi, J. S., and Cho, S. (2015). An analysis of scene change detection in HEVC bitstream. In *IEEE ICSC*, pages 470–474. IEEE.

Hamidouche, W., Raulet, M., and Deforges, O. (2014). Real time SHVC decoder: Implementation and complexity analysis. In *IEEE ICIP*, pages 2125–2129.

Holliman, M. and Chen, Y. K. (2003). Mpeg decoding workload characterization. In *CAECW Workshop*.

Isovic, D., Fohler, G., and Steffens, L. (2003). Timing constraints of MPEG-2 decoding for high quality video: misconceptions and realistic assumptions. In *Euromicro Conf. on Real-Time Sys.*, pages 73–82. IEEE.

Kim, I.-K., Min, J., Lee, T., Han, W.-J., and Park, J. (2012). Block partitioning structure in the HEVC standard. *Circuits and Systems for Video Technology, IEEE Transactions on*, 22:1697–1706.

Kreku, J., Tiensyrja, K., and Vanmeerbeeck, G. (2010). Automatic workload generation for system-level exploration based on modified GCC compiler. In *DATE Conf.*, pages 369–374.

Krunz, M., Sass, R., and Hughes, H. (1995). Statistical characteristics and multiplexing of MPEG streams. In *INFOCOM*, pages 455–462. IEEE.

Liu, W., Xu, J., Wu, X., Ye, Y., Wang, X., Zhang, W., Nikdast, M., and Wang, Z. (2011). A noc traffic suite based on real applications. In *IEEE ISVLSI*.

Mashat, A. S. (1999). *VBR MPEG traffic: characterisation, modelling and support over ATM networks*. PhD thesis, University of Leeds.

Mendis, H. R. (2015). Analysis data, sourcecode and usage examples of proposed workload generator. http://gdriv.es/hevcanalysisdata.

Mendis, H. R., Audsley, N. C., and Indrusiak, L. S. (2015). Task allocation for decoding multiple hard real-time video streams on homogeneous nocs. In *INDIN conf.*

Mudholkar, G. S., Srivastava, D. K., and Freimer, M. (1995). The exponentiated weibull family: a reanalysis of the bus-motor-failure data. *Technometrics*, 37:436–445.

Multicoreware (2015). x265 HEVC encoder/h.265 video codec. http://x265.org/. [Online; accessed 26-October-2015].

Naccari, M., Weerakkody, R., Funnell, J., and Mrak, M. (2015). Enabling ultra high definition television services with the hevc standard: The thira project. In *IEEE ICMEW conf.*

Opensource (2015). Openhevc HEVC decoder. https://github.com/openhevc/. [Online; accessed 26-October-2015].

Roitzsch, M. and Pohlack, M. (2006). Principles for the prediction of video decoding times applied to MPEG-1/2 and MPEG-4 part 2 video. In *RTSS conf.*

Saponara, S., Denolf, K., Lafruit, G., Blanch, C., and Bormans, J. (2004). Performance and complexity coevaluation of the advanced video coding standard for cost-effective multimedia communications. *EURASIP J. Appl. Signal Process.*, pages 220–235.

Soares, A. B., Bonatto, A. C., and Susin, A. A. (2013). Development of a soc for digital television set-top box: Architecture and system integration issues. *International Journal of Reconfigurable Computing*.

Sullivan, G., Ohm, J., Han, W.-J., and Wiegand, T. (2012). Overview of the high efficiency video coding (HEVC) standard. *IEEE TCSVT journal*, 22(12):1649–1668.

Tanwir, S. and Perros, H. (2013). A survey of VBR video traffic models. *IEEE Communications Surveys Tutorials*, pages 1778–1802.

Wu, H., Claypool, M., and Kinicki, R. (2005). Guidelines for selecting practical MPEG group of pictures. In *In Proceedings of IASTED (EuroIMSA) conf.*

Yuan, W. and Nahrstedt, K. (2002). Integration of dynamic voltage scaling and soft real-time scheduling for open mobile systems. In *NOSSDAV workshop*.

Zach, O. and Slanina, M. (2014). A comparison of H.265/HEVC implementations. In *ELMAR, 2014*.